Eur. Phys. J. D **14**, 83–88 (2001)

THE EUROPEAN PHYSICAL JOURNAL D

EDP Sciences

Phase transitions in Co nanoclusters grown by pulsed laser deposition

V. Dureuil, C. Ricolleau[a], M. Gandais, and C. Grigis

Laboratoire de Minéralogie-Cristallographie de Paris[b], Universités Paris 6 et Paris 7, case 115, 4 place Jussieu, 75252 Paris Cedex 05, France

Received 03 July 2000 and Received in final form 22 December 2000

Abstract. The crystalline structure of Co clusters embedded in an amorphous Al_2O_3 matrix was studied by transmission electron microscopy (TEM) and electron diffraction (TED). In the first stage of the growth a metastable structure (body-centred-cubic) is observed. A face-centred-cubic phase (fcc) is found when the size of the clusters increases (diameter > 4 nm). The hexagonal-close-packed phase arises in the fcc phase by a succession of stacking faults at the largest sizes. The mechanisms of phase transformation have been determined by using high resolution electron microscopy (HREM). The chemical nature of the clusters, in particular the existence of Co–O bonds, was investigated by using electron energy loss spectroscopy (EELS).

PACS. 61.46.+w Nanoscale materials: clusters, nanoparticles, nanotubes, and nanocrystals – 61.16.Bg Transmission, reflection and scanning electron micrography (including EBIC) – 61.50.Ks Crystallographic aspects of phase transformations; pressure effects

1 Introduction

Nanocomposite materials, which consists of metallic nanoclusters dispersed in a dielectric, have regained much attention because of the possibility of achieving very large third-order non-linear susceptibility $\chi^{(3)}$ in the range 10^{-7} to 10^{-8} esu [1], and fast non-linear response time τ in the picosecond time frame [2]. The composite structures investigated thus far have a formulation M: dielectric, where M is a noble metal: Ag, Au and Cu, or a transition metal and the dielectric is an oxide: SiO_2 [3], Al_2O_3 [4], TiO_2 [5] for example, or a glass [6]. These materials, most attractive for optical device applications, may offer a solution for the fabrication of the multigigabit switch/routers made necessary to support the traffic of the future telecommunication networks. Today however, the non-linear optical properties of these composites peak in the visible spectrum, *i.e.* typically in the wavelength range which corresponds to the surface plasmon resonance frequencies of the quasi-spherical metallic clusters. The use of nanocomposites in the wavelength range 1.3–1.55 μm requires the development of metallic, noble or transition metals, nanoclusters in the shape of elongated ellipsoids.

One of the candidate composites is the Co: amorphous Al_2O_3 (a-Al_2O_3) system, where Co particles may be shaped *ex situ* in a magnetic field. In that case, the ellipsoidal shape will be favoured owing to the competition between surface energy and demagnetizing field energy [7].

This work reports on the structural study, made by transmission electron microscopy (TEM), of the Co nanoclusters embedded in Al_2O_3 films. The preparation of the samples and the results of TEM analyses are presented in succession.

2 Experimental

The Al_2O_3/Co/Al_2O_3 films, produced by the pulsed laser-assisted deposition (PLD) technique, were directly deposited on a carbon film supported by a copper grid for transmission electron microscopy analyses. The laser was an excimer laser (Lambda Physik LPX 325i) with a wavelength of 248 nm (KrF) and a 30 ns full width half maximum (FWHM) pulse duration. The Al_2O_3 and Co targets were mounted on a computer-controlled target holder, thus allowing the alternate deposition of Al_2O_3 and Co films. The background pressure in the growth chamber was 3.5×10^{-6} mbar. The films of the Al_2O_3/Co/Al_2O_3 structure were deposited with the same conditions, namely: a pulse repetition of 2 Hz, a laser fluence of about 2.3 J/cm^2 and a target-substrate distance of 5 cm. An estimate of the film temperature during deposition was 430 °C, which yielded relatively dense amorphous alumina as inferred from the measured refractive index of test samples: $n = 1.66$, as compared to the crystallised alumina obtained at 600 °C: $n = 1.7$. The cooling rate was 10 °C/min until ∼120 °C, when the sample was extracted from the deposition chamber.

[a] e-mail: ricollea@lmcp.jussieu.fr
[b] UMR 7590 du CNRS

Table 1. Evolution of the mean size, the standard deviation and the particle density as a function of the effective Co thickness.

N° samples	Mean diameter (nm)	Standard deviation (nm)	Particle density ($/10^{-2}$ μm^2)
N° 1: 250 pulses (0.1 nm)	1.6	0.41	268
N° 2: 500 pulses (0.3 nm)	3.4	0.50	141
N° 3: 1 000 pulses (0.7 nm)	4.5	1.19	122
N° 4: 2 000 pulses (1.4 nm)	11.0	2.53	40
N° 5: 4 000 pulses (2.8 nm)	21.1	5.20	16

Table 2. Lattice parameters of the Co-bcc, Co-fcc and γ-Al_2O_3 phases.

bcc-Co d_{hkl} / (hkl) indexes	fcc-Co d_{hkl} / (hkl) indexes	γ-Al_2O_3 d_{hkl} / (hkl) indexes
1.99 Å / (110)	2.05 Å / (111)	2.39 Å / (311)
1.41 Å / (200)	1.77 Å / (200)	1.98 Å / (400)
1.15 Å / (211)	1.25 Å / (220)	1.40 Å / (440)

The effective thickness of the cobalt layer sandwiched between the Al_2O_3 layers was doubled from run to run, starting from typically 0.1 to 2.8 nm (250 to 4 000 pulses). It was calibrated by means of the RBS technique. The thickness of the Al_2O_3 layers were 10 nm for the substrate and 20 nm for the coating. The deposition times of these films ranged from 15 min to 46 min, according to the pulse number.

The structural parameters of the Co phases were determined by using High Resolution TEM (HREM) and Transmission Electron Diffraction (TED). The HREM observations were made on a Topcon 002B electron microscope operating at 200 kV, with a point to point resolution of 0.18 nm. The TED experiments were made on the Jeol 2000 FX electron microscope.

Cobalt being easily oxidable, the chemical nature of the clusters was analysed by electron energy loss spectroscopy (EELS). EELS analyses were performed on a Philips CM 20 microscope operating at 160 kV and equipped with a GATAN parallel detector spectrometer. The energy resolution was 1.5 eV in the experimental conditions used for the analysis.

3 Results

The cobalt occurs as dispersed and randomly oriented clusters on the a-Al_2O_3 film. The cluster formation is not surprising since it is well known that Co has a low wetting coefficient on Al_2O_3 (Fig. 1a) [8]. The mean diameter of the clusters with the standard deviation and the number of clusters per unit area are given in Table 1 as a function of the cobalt effective thickness. After the first stage of growth, the particle density (number of particles per unit area) decreases continuously as the effective thickness increases, which indicates the coalescence of clusters.

For the two thinnest samples (250 and 500 pulses corresponding to 0.1 and 0.3 nm of cobalt respectively), the lattice parameters measured by TED (Fig. 1b) are in full agreement with a Co body-centered-cubic (bcc) structure having a cell parameter $a_0 = 2.87 \pm 0.05$ Å. The bcc structure is not a stable form for cobalt. The a_0 value measured in our experiments is close to the theoretical values found earlier [9,10].

The thicker film obtained with 1 000 pulses (0.7 nm of cobalt) represents the stage where a face-centred-cubic (fcc) structure appears and where the occurrence of the Co bcc structure has decreased (Fig. 1b).

At 0.7 nm, which corresponds to a larger deposition time, the matrix is no more completely amorphous but partially composed of small crystallites of γ-Al_2O_3. This complicates the TED pattern since alumina crystallites give rise to (400) and (440) rings respectively close to the (110) and (200) rings of bcc-Co (Tab. 2). Nevertheless, there is one characteristic ring of Co which is distinct from the alumina rings, namely (211). This ring has almost completely disappeared on the diffraction pattern, which indicates the minor presence of the bcc structure relatively to the fcc structure. The coexistence of bcc and fcc structures in a cluster can be seen in HREM where a core shell-like morphology is observed (Fig. 2). The power spectrum (= |Fourier transform|^2) of the digitalised image of this cluster reveals a shell with a Co-fcc structure oriented with the [011]-type direction nearly parallel to the electron beam (inset in Fig. 2). This orientation shows $(11\overline{1})_{fcc}$ and $(\overline{1}1\overline{1})_{fcc}$ planes intersecting with an angle of 70.5°. $(111)_{fcc}$ lattice parameter is equal to 2.05 Å. Concerning the core, the lattice parameter has been measured precisely by using the $(11\overline{1})_{fcc}$ lattice parameter of the shell as a standard. It has been found to be equal to 1.99 Å, in agreement with the $(01\overline{1})_{bcc}$ lattice spacing. The angle between $(11\overline{1})_{fcc}$ and $(01\overline{1})_{bcc}$ inside the cluster has been found to be equal to about 10°. This value will be discussed in the next section. HRTEM also shows Co-hcp nanoparticles in small amount. They are facetted and they grow with an anisotropic shape with the long axis parallel to {0002} (Fig. 3). This shape looks very similar to the Wulff polyhedron, delimited by (001) and

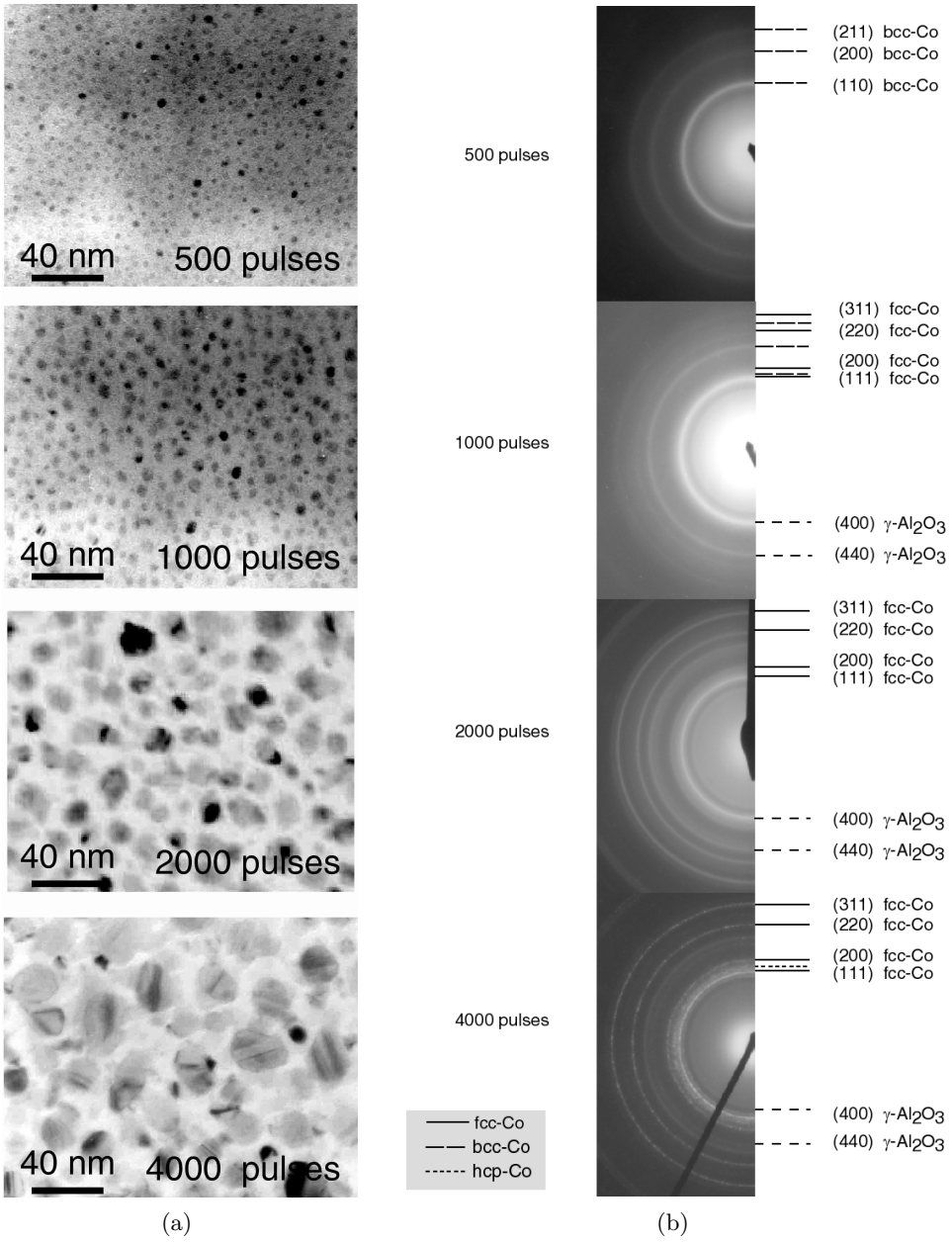

Fig. 1. (a) TEM bright field images of cobalt films having a nominal thickness of 0.3 to 2.8 nm of cobalt encapsulated in a-Al_2O_3 and (b) electron diffraction pattern of the corresponding films.

(011) faces [11,12]. We must notice that the fcc structure is the stable form of bulk cobalt at high temperature (*i.e.* $T \geq 430$ °C), and the hexagonal close packed one (hcp) is stable at lower temperature.

The Co-fcc structure is also principally found by both TED and HREM in the film obtained at 1.4 nm of Co (Fig. 1b). The Co nanoparticles are still isolated and are mostly single crystals that often contain twins and stacking faults. These defects are well known to frequently occur in Co-fcc, since there is no distortion of the nearest neighbour bonds at stacking faults and twin boundaries [13].

At 2.8 nm (Figs. 1a and 1b), the crystalline structure is still in majority fcc but the electron diffraction pattern indicates also the existence of hcp structure. The majority of the clusters seen by HREM exhibits either a Co-fcc structure with stacking faults and twins boundary or even a two phase mixture, where the Co-fcc and Co-hcp domains share a close packed atomic layer as shown in Figure 4. A small number of particles with a pure hcp structure are also observed. We may notice that even at 3.5 nm,

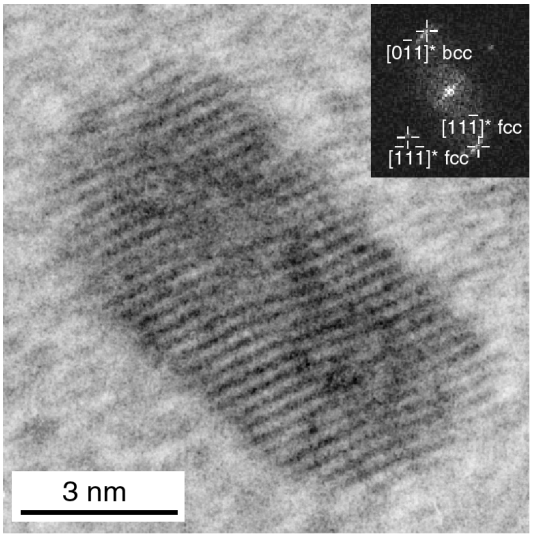

Fig. 2. HREM image and FT (inset) showing the core-shell-like structure of Co clusters (sample N° 3). The core is bcc and the shell is fcc.

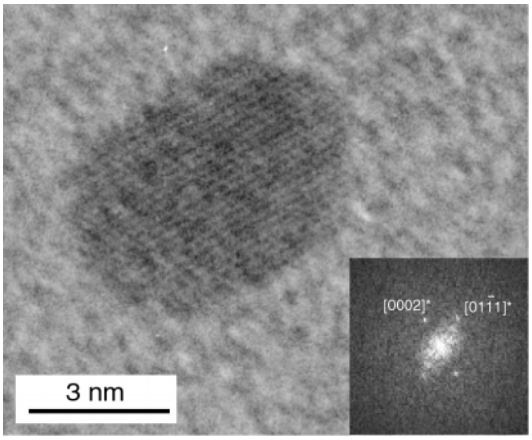

Fig. 3. HREM image and FT (inset) of an anisotropic cluster with close-packed hexagonal structure (sample N° 3).

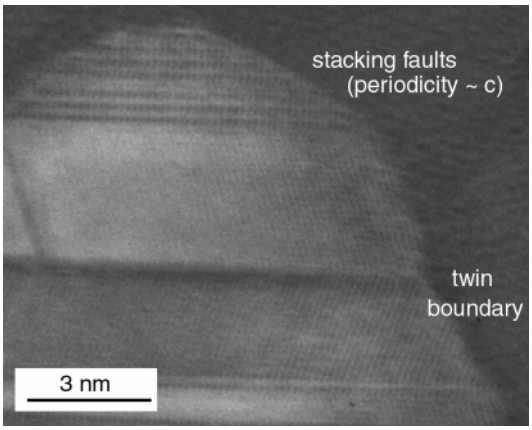

Fig. 4. HREM image of a cobalt cluster with different kind of faults: twin boundary and stacking faults (sample N° 5). The succession of stacking faults with a periodicity about **c** (lattice parameter of hcp-Co) induces a transformation from fcc to hcp.

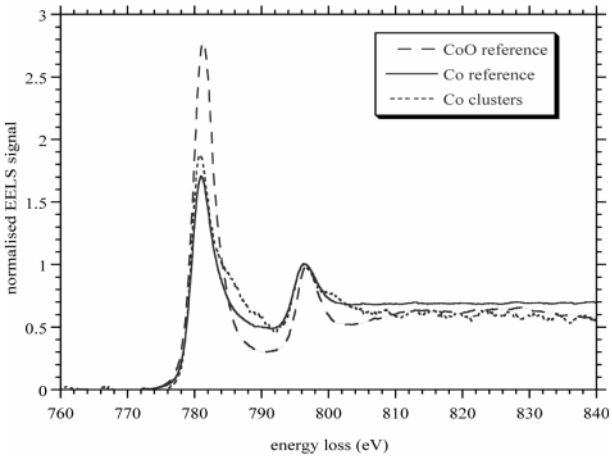

Fig. 5. EELS spectra at the $L_{2,3}$ edge of Co, after background subtraction and normalisation at the L_2 peak. Solid line: Co reference; dashed line: CoO reference; dotted line: Co clusters (0.3 nm nominal thickness of cobalt).

the cobalt layer is composed of clusters, with a size of about 100 nm and principally in the fcc stucture.

EELS analyses have been performed at the $L_{2,3}$ edge of Co in order to have a better knowledge of the chemical bonds involved in the clusters. The $L_{2,3}$ profile exhibits two white lines labelled L_2 and L_3 that correspond to the excitation from the spin-orbit split levels $2p_{3/2}$ and $2p_{1/2}$ respectively. For the $3d$ elements it is known that the relative intensities I_{L3} and I_{L2} of the L_3 and L_2 peak depend on the valence state: the I_{L3}/I_{L2} ratio is significantly higher in the oxide than in the pure elements [14,15]. The I_{L3}/I_{L2} value can thus be used as an indicator of the amount of Co–O bonds.

For the experiment two reference samples have been used. The first reference was a cobalt film, prepared by thermal evaporation from a Co filament of high purity (99.99%) in high vacuum ($\sim 10^{-10}$ mbar). It was deposited on a carbon film supported by a TEM copper grid. The cobalt film was coated *in situ* by a continuous copper film in order to prevent the oxidation of cobalt at further exposure to air. The second reference was a cobalt layer exposed to air without coating. The reference samples give electron diffraction patterns characteristic of fcc-Co and fcc-CoO respectively. Their EELS spectra are presented in Figure 5. For the comparison, the background was substracted and the spectra were normalised at the L_2 peak. The characteristic differences of the pure element and the oxide are well seen. The ratio of the peak heights is larger for the CoO reference ($I_{L3}/I_{L2} = 2.82$) than for the Co reference ($I_{L3}/I_{L2} = 1.70$). Moreover, the intensity after the L_3 peak falls nearer to the background level for CoO than for Co. Concerning the Co clusters, a typical example spectrum is shown in Figure 5. It corresponds to one of the thinnest sample (0.3 nm thick) in which the bcc structure was found. The spectrum is very close to that of the Co reference. However, in spite of noise due to the small amount of cobalt, we can see that the ratio of the peak height is slightly larger ($I_{L3}/I_{L2} = 1.83$) than in the

spectrum of the Co reference. The presence of a small amount of Co–O bonds may be assumed.

4 Discussion

The present work has shown that cobalt clusters occur in a metastable bcc structure for sizes below or equal to 4 nm. Other works have shown that the metastable bcc structure is stabilised in thin film by pseudomorphic epitaxy on suitable substrate, the stability being induced by elastic energy due to the differences of lattice parameters between both materials [16,17]. In the present case, the combination of different factors such as the energy of the species impinging on the film surface (incident species velocity $\sim 10^5$ cm s^{-1}), the high instantaneous deposition rate, the temperature, the presence of impurities, associated to surface energy effects could favour the crystallisation of Co clusters in the bcc structure at small sizes.

Among the different factors mentioned above the effect of oxygen impurity may be envisaged.

The EELS analyses indicate the presence of a small amount of Co–O bonds. The presence of oxygen within the Co clusters cannot be excluded, although the lattice parameters correspond to Co at the accuracy of the measurements in the diffraction patterns. In the smallest clusters, the lattice parameters are very close to those of bcc-Co predicted theoretically. In the larger clusters, they correspond to those of the fcc-Co. We may thus assume that the presence of small amounts of oxygen within the clusters does not modify the crystalline structure of Co but may favour the bcc-structure in the smallest nanoparticles.

The critical size, above which the fcc structure occurs, depends upon growth conditions. It is around 4 nm, in the present experiments. The transformation from a bcc to a fcc structure, so-called Bain transformation, has been thoroughly studied in the past [9,18]. It has been described as induced by a process of elastic lattice deformation. The crystallographic relationship between the two lattices is such as the [001]-fcc axis is parallel to the [001]-bcc axis and the [100]-fcc axis is parallel to the [110]-bcc direction. The transformation involves stretches along the bcc unit cell axis according to the following relations:

$$\lambda_3 = 2^{1/2}\lambda_1 \ (= 2^{1/2}\lambda_2) \tag{1}$$

where λ_1, λ_2 and λ_3 are defined by the ratio a_i/a_{bcc}, a_i being the value of the elongated axis in the direction $\mathbf{i}$ ($i = 1, 2, 3$). For a transformation along a constant atomic volume path, the stretch is:

$$\lambda_3 = (\lambda_1)^{1/2} \ (= (\lambda_2)^{1/2}). \tag{2}$$

In consequence of (1) and (2) the fcc state is reached at $\lambda_3 = 2^{1/3}$ and $\lambda_1 = \lambda_2 = 2^{-1/6}$. In the transformation, $(01\overline{1})_{\mathrm{bcc}}$ becomes $(11\overline{1})_{\mathrm{fcc}}$ with an angle of 9.7°, according to the angle between the vector $\mathbf{v} = \mathbf{a}_2 - \mathbf{a}_3$ normal to $(01\overline{1})_{\mathrm{bcc}}$ and the vector $\mathbf{u} = a_{\mathrm{fcc}}/a_{\mathrm{bcc}}(\sqrt{2}\,\mathbf{a}_2 - \mathbf{a}_3)$ normal to $(11\overline{1})_{\mathrm{fcc}}$ (Fig. 6). The agreement between the value of 9.7° derived from the above calculation and the value of 10° measured in the cluster shown in Figure 2 suggests that the transformation from bcc to fcc structure in the cluster has been produced by the mechanism described in the theory of Bain transformation. The bcc → hcp transformation has been described by the same process associated to some additional shears [19].

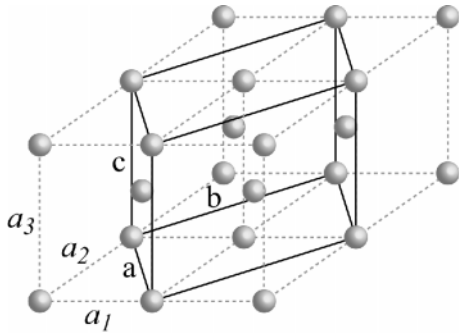

Fig. 6. Scheme of the bcc and fcc Co structures showing the crystallographic relationship between both structures. Plain line: fcc lattice frame – dashed line: bcc lattice frame. a_1, a_2, a_3 are the stretch basis vectors of the bcc structure.

Above the critical size mentioned previously, the structure of Co found in the film is fcc, the high temperature form of bulk Co and not hcp. This state could be explained by two factors. At first, the fcc occurrence in clusters may be ascribed to lower surface energy. In previous works, Co nanoparticles with a fcc structure have been observed at low temperature [20–23]. Moreover, the film temperature (430 °C) during deposition is close to the hcp → fcc transition temperature (420 °C), which permits the coexistence of the two structures.

The hcp phase arises in the fcc phase by succession of twin boundaries and/or stacking faults in the fcc structure. Indeed, the fcc and hcp structures are close to each others. They differ by the stacking sequence of the close packed atomic layers ABCABCABC for fcc and ABABAB for hcp. Thus, the two phase structures could be formed by stacking faults and/or twin boundaries in the fcc structure. In the last sample (4 000 pulses), the particles are mainly Co-fcc, but they exhibit the Co-hcp stacking sequences associated to the existence of faults. Figure 4 illustrates this situation: the core of the cluster is Co-fcc, but on an extremity of the cluster stacking faults are observed. These stacking faults have roughly a **c** period, which gives the hcp crystalline structure. The orientational relationship between both structures are: $(111)_{\mathrm{fcc}} \parallel (0001)_{\mathrm{hcp}}$ and $\langle 110\rangle_{\mathrm{fcc}} \parallel \langle 11\,\overline{2}\,0\rangle_{\mathrm{hcp}}$, which is well known in this phase transformation.

5 Conclusion

The study of cobalt in a-Al_2O_3 deposited by PLD reveals very interesting behaviours. The cobalt forms islands on a-Al_2O_3. The particle density (number of particles per unit area) decreases continuously as the effective thickness increases indicating the coalescence of clusters during the

deposition. The coalescence process is induced by diffusion of atoms and small clusters on the heated a-Al_2O_3 substrate ($T = 430$ °C).

The crystalline structure changes according to the size of the clusters. In the first stage of the nucleation and growth process (until 4 nm), the cobalt has a metastable body-centred-cubic structure, probably favoured by the presence of a small amount of oxygen in the Co clusters. Further experiments are needed in order to determine more precisely if others parameters are at the origin of the occurrence of this Co-bcc phase. When the size of nanoparticles increases the crystalline structure transforms into face-centred-cubic. At larger sizes, the transition fcc → hcp by successions of stacking faults in the fcc structure is locally observed.

This work has been supported by E.U. funds under BRITE EURAM project 98-0616. The authors are grateful to Christian Belouet from Alcatel CRC for fruitful discussions and are indebted to the CECM (Centre d'Études de Chimie Métallurgique) at Vitry-sur-Seine and ECP (École Centrale de Paris) for the use of electron microscope facilities (HREM and EELS respectively).

References

1. D. Ricard, Ph. Roussignol, C. Flytzanis, Opt. Lett. **10**, 511 (1985).
2. C. Flytzanis, F. Hache, M.C. Klein, D. Ricard, Ph. Roussignol, Progr. Opt. **29**, 323 (1991).
3. R.H. Magruder, R.F. Haglund, L. Yang, J.E. Wittig, R.A. Zuhr, J. Appl. Phys. **76**, 708 (1994).
4. J.M. Ballesteros, R. Serma, J. Solis, C.N. Afonso, A.K. Pedford-Long, D.H. Osborne, R.F. Haglund, Appl. Phys. Lett. **71**, 2445 (1997).
5. H.B. Liao, R.F. Xiao, H. Wang, K.S. Wong, G.K.L. Wong, Appl. Phys. Lett. **72**, 1817 (1998).
6. T. Tkizaki, A. Nakamura, S. Kaneko, K. Uchida, S. Omi, H. Tanji, Y. Asahara, Appl. Phys. Lett. **65**, 941 (1994).
7. L. Néel, C.R. Acad. Sci. **225** ,109 (1947).
8. C.T. Campbell, Surf. Sci. Rep. **27**, 1 (1997).
9. P. Alippi, P.M. Marcus, M. Scheffler, Phys. Rev. Lett. **78**, 3892 (1997).
10. A.Y. Liu, D.J. Singh, Phys. Rev. B **47**, 8515 (1993).
11. O. Kitakami *et al.*, Phys. Rev. B **56**, 13849 (1997).
12. R. van Hardeveld, F. Hartog, Surf. Sci. **15**, 189 (1969).
13. J.P. Hirth, J. Lothe, *Theory of dislocations*, 2nd edn. (Krieger Publishing Compagny 1982).
14. R.D. Leapman, L.A. Grunes, P.L. Fejes, Phys. Rev. B **26**, 614 (1982).
15. C. Colliex, T. Manoubi, C. Ortiz, Phys. Rev. B **44**, 11402 (1991).
16. G.A. Prinz, Phys. Rev. Lett. **54**, 1051 (1985).
17. S.K. Kim, C. Pelersen, F. Jona, P.M. Marcus, Phys. Rev. B **51**, 5421 (1995).
18. F. Milstein, H.E. Fang, J. Marschall, Phil. Mag. A **70**, 621 (1994).
19. A.Y. Lui, D.J. Singh, Phys. Rev. B **47**, 8515 (1993).
20. R.M. Wentzcovitch, M.L. Cohen, Phys. Rev. B **37**, 5571 (1988).
21. M. Ohnuma, K. Hono, E. Abe, S. Mitani, H. Fujimori, J. Appl. Phys. **82**, 5646 (1997).
22. J.L. Maurice, J. Briatico, J. Carrey, F. Petroff, L.F. Schelp, Phil. Mag. A **79**, 2931 (1999).
23. V. Dupuis, J. Tuaillon, B. Prevel, A. Perez, P. Melinon, G. Guiraud, F. Parent, L.B. Steren, J. Magn. Magn. Mater. **165**, 42 (1997).